Sustainable Cities and Society 8 (2013) 31–41

Contents lists available at SciVerse ScienceDirect

Sustainable Cities and Society

journal homepage: www.elsevier.com/locate/scs

Methodology for estimating solar potential on multiple building rooftops for photovoltaic systems

Jeffrey B. Kodysh [a], Olufemi A. Omitaomu [a,b,*], Budhendra L. Bhaduri [a], Bradley S. Neish [a]

[a] Computational Sciences and Engineering Division, Oak Ridge National Laboratory, Oak Ridge, TN, USA
[b] Department of Industrial and Systems Engineering, University of Tennessee, Knoxville, TN, USA

ARTICLE INFO

Keywords:
Solar radiation
Irradiation
LiDAR
Hemispherical viewsheds
GIS
Photovoltaic system

ABSTRACT

In this paper, a methodology for estimating solar potential on multiple building rooftops is presented. The objective of this methodology is to estimate the daily or monthly solar energy on individual buildings in a city/region using light detection and ranging (LiDAR) data and a geographic information system (GIS) approach. Conceptually, the methodology is based on the upward-looking hemispherical viewshed algorithm, but applied using an area-based modeling approach. The methodology considers input parameters, such as surface orientation, shadowing effect, elevation, and atmospheric conditions that influence solar intensity on the earth surface. The methodology has been implemented for some 212,000 buildings in Knox County, Tennessee, USA. Based on the results obtained, the methodology seems to be adequate for estimating solar radiation on multiple building rooftops. The use of LiDAR data improves the radiation potential estimates in terms of the model predictive error and the spatial pattern of the model outputs. This methodology could help cities/regions interested in sustainable projects to quickly identify buildings with higher potentials for roof-mounted photovoltaic systems.

1. Introduction

Many cities across the world are encouraging the use of solar energy technologies in promoting the concept of sustainable cities. The active and passive applications of solar energy could effectively transform neighborhoods, commercial districts, and urban areas into small, localized power plants. An active application will include the use of photovoltaic (PV) for electricity generation in a distributed style of generation; and a passive application will include designing buildings and windows to use solar energy in a sustainable manner. In the United States, for instance, the Department of Energy (DOE) is promoting large scale deployment of roof-mounted PV systems for electricity generation in residential and commercial buildings. In most cases, both the solar resources and roof space required are available. As an illustration, the United States has about 150 billion square feet of residential roof space and about 50 billion square feet of commercial roof space (Hoff, 2009, p. 21) – a significant and untapped resource for the deployment of PV systems. Roof-mounted PV systems eliminate extensive transmission lines connection because they are installed closer to load; reduce/eliminate land investment because the buildings are already built; are less vulnerable to vandalism because they are not in isolated areas; and can be more esthetically appealing to the neighbors than some of the other distributed renewable options, such as wind. With the aspiration to increase the number of roof-mounted PV systems, there is a need to identify buildings in a region with higher potentials for PV installations, and assess their potential electricity yield. This identification process must be faster, easier, and should reduce the number of individual onsite studies/visits than current estimation techniques. The lack of daily/monthly solar radiation data for each building, however, is limiting the identification process, and thus the assessment of potential electricity yield of roof-mounted PV installations in a region. The availability of *building rooftop solar potential data* could offer a powerful way for characterizing buildings in a region. Such data could also be used to generate solar potential maps for roof-mounted PV applications.

Solar potential maps have been developed for concentrated solar thermal and concentrated PV applications. For example, the National Renewable Energy Laboratory (NREL) maintains a series of solar potential maps for concentrated solar thermal and concentrated PV plants in the United States. However, the data used to generate these maps are not suitable for roof-mounted PV applications because the spatial resolution of the data is usually low (about 1 km) compared to what is required for roof-mounted applications. Furthermore, the process for generating the data does not account for location specific characteristics, such as roof slope and aspect and shadowing effects, that are critical to roof-mounted PV systems. To enhance the modeling of solar

* Corresponding author at: 1, Bethel Valley Road, Oak Ridge, TN 37831-6017, USA.
E-mail addresses: omitaomuoa@ornl.gov, femiomit@gmail.com (O.A. Omitaomu).

2210-6707/$ – see front matter © 2013 Elsevier B.V. All rights reserved.
http://dx.doi.org/10.1016/j.scs.2013.01.002

potential for roof-mounted PV applications, some GIS-based tools have been developed. These tools include *In My Backyard* (IMBY) available at http://mercator.nrel.gov/imby/, PVWatts available at http://www.pvwatts.org, and CH2MHill (2008). However, these tools are geared toward introducing homeowners to the possible benefits of PV systems, and are only suitable for individual building assessment. The tools provide users the ability to estimate solar potential on a building, and compare the calculated electricity potential to the electricity consumption for the building. However, the tools are not applicable for estimating solar potential for multiple buildings in an efficient and cost effective manner. Furthermore, the tools do not account for building-specific characteristics, such as trees and adjacent buildings, that could impact the solar potential estimation.

Significant progress has also been made in the last two decades toward developing solar radiation models using analytical, numerical simulation, statistical, and artificial intelligence approaches. Some of the recent models are developed by Sen and Sahin (2001), Adnan, Arcaklioglu, Ozalp, and Caglar (2001), Tymvios, Jacovides, Michaelides, and Scouteli (2005), Mellit, Benghanem, Hadj Arab, and Guessoum (2005), López, Batlles, and Tovar-Pescador (2005), Elminir, Azzam, and Younes (2007) and Mubiru and Banda (2008). The majority of these models require a large number of empirically determined parameters, which is usually a challenge especially in areas where measurement instruments are not available. In addition, these models need to assume some behavior of the ground-truth data even though location-specific data varies from one building to another. As a result, the models present significant challenges in modeling solar potential for a long term; or for prediction in areas where measurement instruments are not available; or where there are missing data in the input database. In some cases, the computational time required for training the model for accurate prediction is usually significant.

There have also been some GIS-based models developed in the last two decades. An advanced model for ecological and biological applications developed by Fu and Rich (2000) was implemented as an Environmental Systems Research Institute's (ESRI's) ArcMap GIS Extension, known as the Solar Radiation Toolset. This model generates an upward-looking hemispherical viewshed based on a digital terrain model and is suitable for fine scale studies. This model forms the basis for the proposed methodology in this paper. The *SRAD* model (Wilson and Gallant, 2000) was designed to model topo- and mesoscale processes of the landscape; however, the calculation of solar radiation over large territories is limited. Suri and Hofierka (2004) developed a solar radiation model called *r.sun* within the GRASS GIS environment. Other recent computational solar radiation models are presented by Hofierka and Kanuk (2009), Suri, Huld, Dunlop, and Hofierka (2007), Suri, Huld, and Dunlop (2005), Neteler and Mitasova (2004), Gadsden, Rylatt, and Lomas (2003) and Hammer et al. (2003).

In this paper, a GIS-based methodology that accounts for individual building characteristics is presented for estimating solar potential on multiple building rooftops. Our contributions in this paper are: (i) the extension of the upward-looking hemispherical rooftop solar radiation model for solar radiation modeling over a large area; (ii) the development of roof-mounted solar radiation map at a higher resolution of about 1 m horizontal resolution and about 0.3 m vertical resolution; and (iii) the development of a methodology for estimation of solar potential on multiple buildings for roof-mounted PV systems.

The remainder of this paper is organized as follows. Section 2 describes the light detection and ranging (LiDAR) data used as input in the proposed methodology, and the upward-looking hemispherical viewshed algorithm that is the basis for the proposed methodology. Section 3 presents the proposed methodology for estimating rooftop solar radiation potential on multiple buildings. Section 4 discusses the results and some of the insights from the application of this methodology to some 212,000 buildings in Knox County, Tennessee, USA. A short summary concludes the paper in Section 5.

2. The input data and the upward-looking hemispherical viewshed algorithm

In this section, a description of the LiDAR data used as input for the proposed methodology and the procedure for processing the data is provided. Furthermore, to provide readers an introduction to the algorithm for modeling solar radiation potential, the upward-looking hemispherical viewshed algorithm is also briefly described.

2.1. LiDAR-based digital elevation models (DEMs)

The light detection and ranging system is a remote sensing technology used to collect topographic data of the features on the earth's surface, including natural and man-made features. The LiDAR data can be collected by an airborne or a ground-based system. Furthermore, it can be used in areas where there are no infrastructures to use a ground-based system. The airborne system involves the use of LiDAR sensors mounted rigidly on-board an aircraft. During a flight, the aerial LiDAR sensors transmit billions of laser light pulses in visible and near infrared wave lengths to the earth's surface. Upon hitting solid objects on the earth's surface, the beams are reflected back to the LiDAR sensors. The time difference between the emission of the laser beam and the return of the reflected laser signal to the aircraft is then recorded. The LiDAR instruments only collect elevation data. To make the data spatially relevant, the positions of the data points must be known. A high-precision GPS antenna is also mounted on the aircraft. As the LiDAR sensors collect data points, the location of the data are simultaneously recorded by the GPS sensor. The end product is accurate, geographically registered longitude, latitude, and elevation positions for every data point. LiDAR has three advantages: it is easy to collect large amount of data without disrupting other activities; it is fast to collect the data because the survey portion of the project is reduced from months to days; and the data collected is of higher accuracy. These advantages have generated lots of interest in the LiDAR system. To this end, many county and state governments, along with private organizations, have collected high-resolution aerial LiDAR data for various urban planning, cadastral mapping, and environmental projects. The widespread availability of high-resolution LiDAR data and LiDAR-derived data products in urbanized areas is a motivation for implementing the proposed methodology.

The raw LiDAR data allow the generation of digital elevation models (DEM) of the ground surface, which in turn is used for solar potential estimation. The process of creating the DEM is beyond the scope of this paper. However, interested readers may see the online ArcGIS Help Library (2011a, 2011b) for additional information about generating a DEM from LiDAR data. An example of processed LiDAR data is shown in Fig. 1. It should be noted that other useful geospatial products, such as, contour maps, slope and aspect maps, building footprints, and three-dimensional buildings for virtual reality visualizations can be obtained from the raw LiDAR data. Even though the raw LiDAR data are typically interpolated into raster DEM of various resolutions, the resolution of the DEM used for estimating rooftop solar potential must accurately reflect the unique characteristics of the roof, such as roof slope, roof orientation, and adjacent structures and vegetation. This is necessary for characterizing all the surface features completely. The horizontal and vertical accuracies of LiDAR have improved in the last few years. It is not uncommon to obtain aerial LiDAR of about 1-m accuracy. Some high priority applications are currently pushing for less

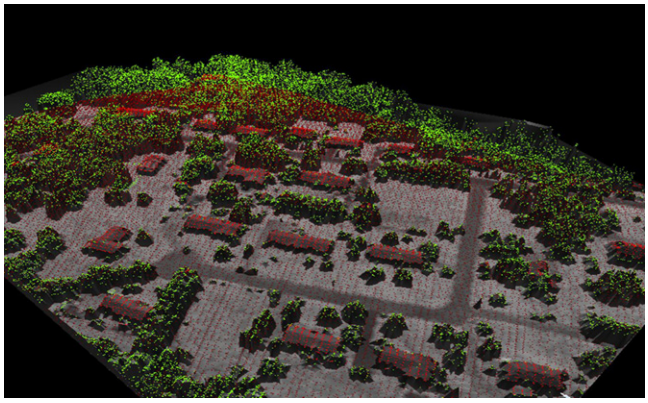

Fig. 1. An example of a high resolution LiDAR data point cloud. Note how vegetation, roads, and buildings are accurately represented in the image.

than 2 cm accuracy. The DEM used for the application in this paper is about 1 m horizontal and 0.3 m vertical accuracy.

2.2. Upward-looking hemispherical viewshed algorithm

Modeling solar potential on building rooftops is a challenging process. Although solar radiation striking the top of the earth's atmosphere is relatively consistent at about 1.367 kW/m^2, the radiation that actually reaches a given rooftop is much more variable. Many factors are responsible for this variation. For instance, seasonal variations in radiation intensity, shading from adjacent topography and surface features, and individual building characteristics, such as, roof size, slope, and orientation, usually impact the final amount of solar radiation that strike an individual rooftop. In addition, weather and other atmospheric considerations also impact the final solar radiation values. To account for these factors and accurately estimate solar radiation potential for a specific location, Fu and Rich (2000) presented a GIS-based upward-looking hemispherical viewshed algorithm for estimating solar radiation potential. Their algorithm is briefly described in this section. Interested readers should see their paper for further details.

The viewshed algorithm calculates sky obstruction and incoming solar radiation for a given location on a DEM. The development of viewshed algorithms for solar radiation estimation techniques stems from research surrounding hemispherical canopy photography, a technique used to measure canopy density. Viewshed algorithms are, in essence, a virtualized version of hemispherical canopy photography. The upward-looking viewshed algorithm implemented in the ESRI's ArcMap *Solar Analyst* toolbox consists of three initial calculations – viewshed, sunmap, and skymap calculation – and one final calculation that uses the results of the initial calculations to estimate a solar radiation value for each location on the DEM. Each step of the calculation is explained in the following subsections.

2.2.1. The viewshed calculation

The viewshed calculation determines which parts of the "sky" are obstructed for a particular location on a DEM. This is achieved by searching in a specified set of directions around a location on the DEM and determining the maximum angle of "sky" obstruction caused by other cells in the DEM. This calculation is based on the premise that cells in the DEM that have a higher elevation relative to another cell will "shade" the lower placed cells. For the unsearched directions, sky obstruction is calculated using interpolation method. One can describe this stage as a process in which an upward-looking hemispherical camera is placed on each cell in a DEM and the camera captures which sky directions are visible and which are obscured. An illustration of the output is shown in Fig. 2a.

Viewsheds are projected into a temporary two-dimensional grid that represents the "sky" for the final solar radiation calculation involving the soon-to-be-built sunmaps and skymap calculations. These temporary grids are upward-looking, hemispherical raster representations of the sky and do not have a geographic coordinate system. Each cell in this temporary grid is assigned a value that corresponds with visible versus obstructed sky direction. The grid cell location, row and column, corresponds to a zenith angle θ (angle relative to the zenith) and an azimuth angle α (angle relative to north) on the hemisphere of directions.

2.2.2. The sunmap calculation

Once a viewshed has been created for a particular cell location on a DEM, the next calculation creates sunmaps, a two-dimensional grid representation that identifies suntracks – the apparent position of the sun as it varies through time for that same location. Sunmaps are used in the final solar radiation calculation to estimate the amount of direct solar radiation a location on the DEM receives. The position of the sun (zenith and azimuth angles) is calculated based on latitude, day of year, and time of day using standard astronomical formulae. Zenith and azimuth angles are projected into two-dimensional grids with the same resolution used for viewsheds. Two sunmaps are created – one to represent periods between the winter solstice and the summer solstice (between

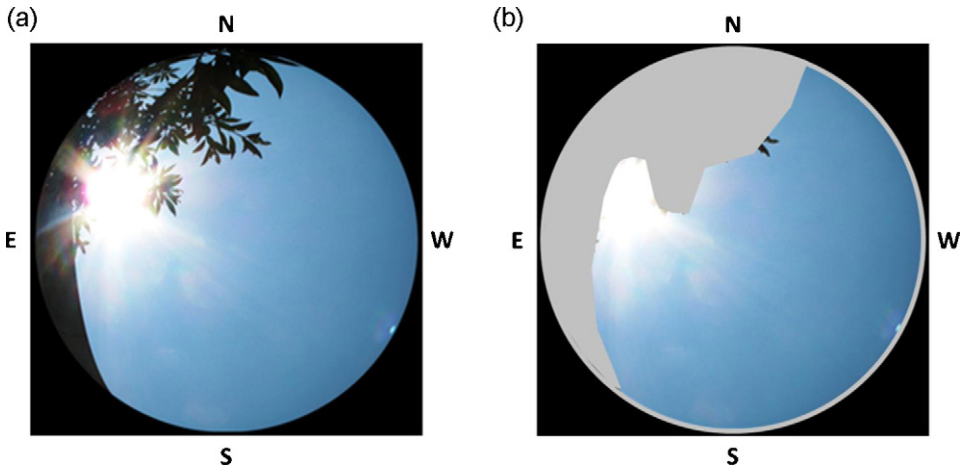

Fig. 2. (a) An example of the image captured by an upward-looking camera; (b) the resulting viewshed for a location with sky directions that are visible (blue area) and obscured (gray area). (For interpretation of the references to color in this figure legend, the reader is referred to the web version of the article.)

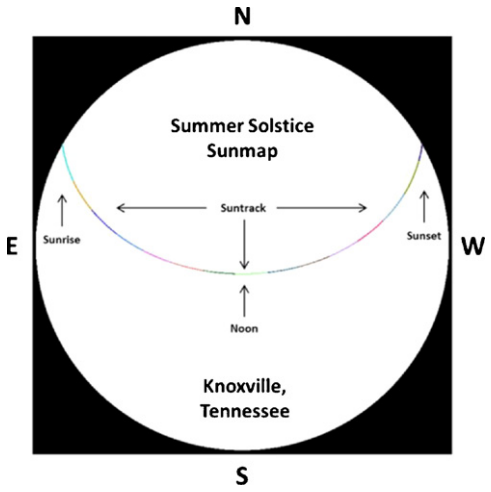

Fig. 3. Sunmap for summer solstice for a day.

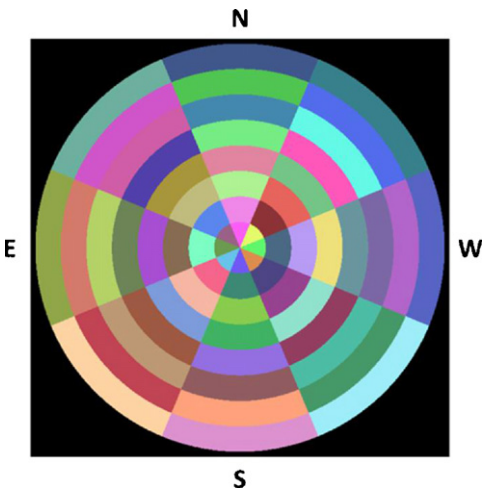

Fig. 4. A summer solstice skymap with sky sectors defined by 8 zenith divisions and 8 azimuth divisions.

December 22 and June 22); and the other to represent periods between the summer solstice and the winter solstice (between June 22 and December 22). Generating a sunmap for every raster cell makes calculation of solar radiation considerably faster. Fig. 3 is an example of the sunmap calculation outputs for summer solstice for a day.

2.2.3. The skymap calculation

The third calculation is the skymap calculation. This calculation divides the entire sky into a series of sky sectors defined by zenith and azimuth divisions. Skymaps are used in the final solar radiation calculation to estimate the amount of diffuse solar radiation at a location on the DEM receives. Sky sectors in the skymap must be small enough so that the centroid zenith and azimuth angles reasonably represent the direction of the sky sector in subsequent calculations. Skymaps, like viewsheds and sunmaps, are also projected into a temporary two-dimensional grid for the solar radiation calculation. A skymap with sky sectors defined by 8 zenith and azimuth divisions respectively is shown in Fig. 4.

2.2.4. The solar radiation calculation

After the three steps described are completed, the outputs are used to calculate the amount of diffuse and direct radiation received by a given location on the DEM. The first stage in this calculation attempts to determine the proportion of unobstructed sky area – or gap fraction – in each skymap or sunmap sector in the temporary two-dimensional grid (that is, to determine which parts of the sunmap and skymap are not obstructed). This is calculated by dividing the number of unobstructed cells by the total number of cells in that sector. An overlay of viewshed (first initial calculation) with sunmap (second initial calculation) and skymap (third initial calculation) respectively is shown in Fig. 5.

Once obstructed sky direction areas have been identified, solar radiation is then calculated based on such factors as gap fraction, sun position, atmospheric attenuation and ground receiving surface orientation. A total solar radiation value is obtained for each location on the topographic surface, thus producing a solar radiation map for the whole area of interest. The total solar radiation or global solar radiation (GR) is the sum of direct and diffuse solar radiation of all sectors.

$$G_R = D_R + F_R \tag{1}$$

where D_R is direct solar radiation for all sunmap sectors and F_R is diffuse solar radiation for all skymap sectors. That is,

$$D_R = \sum DR_{\theta\alpha}$$
$$D_F = \sum DF_{\theta\alpha} \tag{2}$$

The direct solar radiation from a sunmap sector with a centroid at zenith angle θ and azimuth angle α is given as:

$$DR_{\theta,\alpha} = K \times t^{m(\theta)} \times SD_{\theta,\alpha} \times SG_{\theta,\alpha} \times \cos(\beta_{\theta,\alpha}) \tag{3}$$

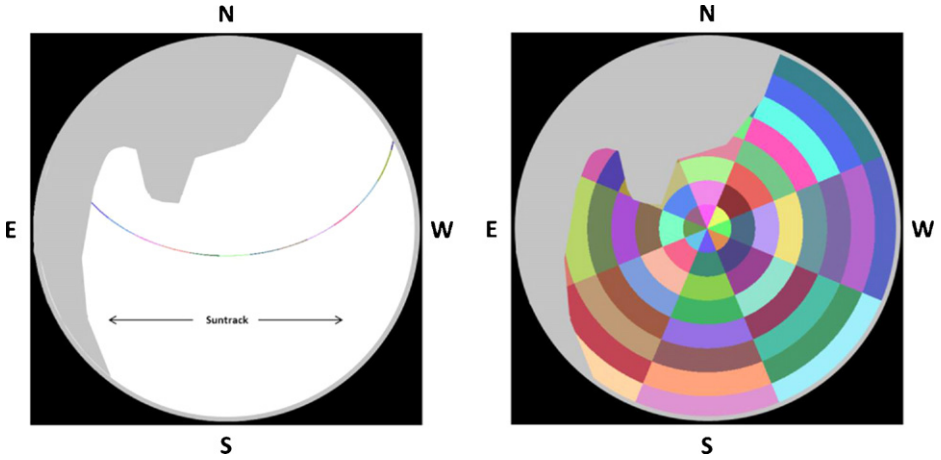

Fig. 5. An overlay of a viewshed on a sunmap (left) and a skymap (right). Shaded areas (gray areas) are obstructed sky directions.

where K is the solar constant and range from 1.338 to 1.368 kW/m^2, but a value of 1.367 kW/m^2 was adopted by the Commission for Instruments and Methods of Observation in 1981; t is transmittivity of the atmosphere for the shortest path in the direction of the zenith; $m(\theta)$ is the relative optical path length; SD is the time duration represented by the sky factor; SG is the gap fraction for the sunmap sector; and $\beta_{\theta\alpha}$ is the angle of incidence between the centroid of the sky sector and the axis normal to the surface. Similarly, the diffuse solar radiation for each sky sector at its centroid is calculated as:

$$DF_{\theta,\alpha} = R_g \times P_d \times D \times SYG_{\theta,\alpha} \times W_{\theta,\alpha} \times \cos(\beta_{\theta,\alpha}) \quad (4)$$

where R_g is the global normal solar radiation; P_d is the proportion of global normal solar radiation flux that is diffused – it is approximately 0.2 for very clear sky conditions and 0.7 for very cloudy sky conditions; D is the time interval for analysis; $SYG_{\theta\alpha}$ is the gap fraction (proportion of visible sky) for the sky sector; $W_{\theta\alpha}$ is proportion of diffuse radiation originating in a given sky sector relative to all sectors; and $\cos(\beta_{\theta\alpha})$ is the angle of incidence between the centroid of the sky sector and the intercepting surface. As an illustration of the implementation of our approach, we used 32 calculation directions with $\theta = 8$ and $\alpha = 8$. We assume a generally clear sky with transmittivity of 0.5, and a corresponding diffuse proportion of 0.3. The day and hour interval for analysis are 14 and 0.5 respectively. The roof slope, aspect, latitude, and longitude data are automatically extracted from the DEM data. It should be noted that the DEM has a specific elevation values above sea level for each cell. Hence, each raster has a slope value, and it is define as the maximum rate of change in value from a particular cell to its eight neighboring raster cells. The sky size for the viewshed, skymap, and sunmap grids is set to 200 cells, which creates 200 × 200 cells. These values are used in all cases described in this paper.

It should be noted that cloud cover, precipitation, dust, and other atmospheric conditions have the ability to markedly reduce, or attenuate, the amount of diffuse and direct solar radiation for a given surface. These atmospheric conditions are constantly changing, and real-time data is usually needed. However, this data is not always available. An alternative approach is to use the so-called average transmittivity value as a surrogate for cloud cover. This is the approach adopted in this model. Transmittivity is a property of the atmosphere and is the ratio of the energy received at the upper edge of the atmosphere to that reaching the earth's surface by the shortest path (in the direction of the zenith), averaged over all wavelengths. Values range from 0 (no transmission) to 1 (complete transmission). Typically, observed values are 0.6 or 0.7 for very clear sky conditions and 0.5 for a generally clear sky (ArcGIS Help Library, 2011a,b). In this model, we used the monthly transmittivity values given on the Gaisma climate website (Gaisma, 2011) for our implementation area.

3. Methodology for estimating solar potential on multiple building rooftops

There are two types of spatial solar radiation models – point-specific models and area-based models. Point-specific models are used for a specific location, and account for the local effect of topography on solar radiation by using empirical relations, visual estimation, or more adequately with the aid of an upward-looking hemispherical algorithm. Point-specific models using an upward-looking hemispherical algorithm have been found to be highly accurate for a given location. Area-based models estimate solar radiation intensity for each cell in an entire geographical area. When coupled with an appropriately created DEM and upward-looking hemispherical viewshed algorithm, area-based spatial models have the ability to account for shading from adjacent topography and surface features, as well as individual building characteristics such as, slope and orientation. Thus, the unique modeling capabilities of area-based spatial solar radiation models are desirable for the creation of highly accurate rooftop solar radiation maps; and these capabilities are explored in the proposed methodology.

The proposed methodology uses the area-based model in ArcGIS and consists of five steps. A flowchart description of the methodology is shown in Fig. 6. In this section, each of the five steps is described in details.

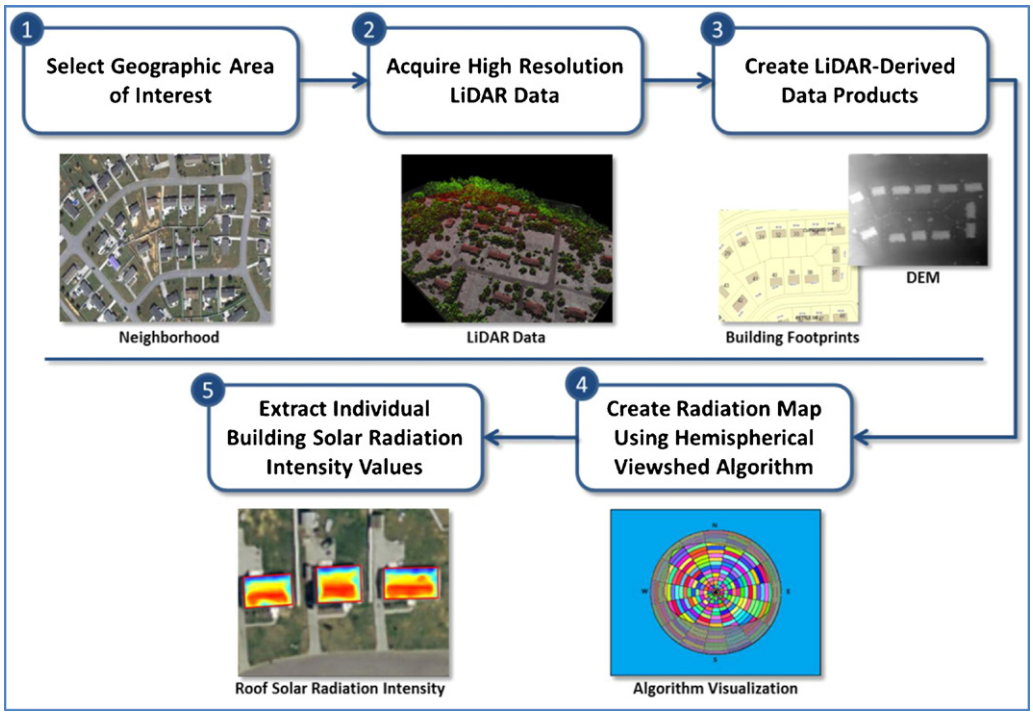

Fig. 6. An overview of the methodology for estimating solar potential on building rooftops.

3.1. The identification of an area of interest

The identification of the area of interest is application dependent. However, such an area of interest may be as small as a few buildings or thousands of buildings. In the application discussed in this paper, our area of interest is all of Knox County, Tennessee, USA. One reason Knox County is of interest is because Knoxville, the largest city in Knox County, is one of the 25 cities selected in 2008 by the U.S. Department of Energy as a Solar America City. Solar America Cities are communities that encourage the use of solar energy technologies. Like many counties in the eastern United States, Knox County does not possess enough solar energy resources that are economically suitable at this time, for centralized solar thermal plants. However, Knox County is still rich in solar energy resources suitable for roof-mounted PV systems. The availability of *building rooftop solar energy data* for Knox County could help spur interest in developing distributed solar energy generation in the county.

Once an area is selected, this step also defines viewshed boundaries around the building rooftops within an area. For a larger area of interest, the implementation of the upward-looking hemispherical viewshed algorithm is computationally intensive; hence, it is important to eliminate features within the area that are not of importance to the computation. These features include roads, farmland, forest, grass, and pavement. The idea is to focus on calculating solar radiation values for the buildings within the area and the adjoining features that could impact the solar insolation values on these buildings. This approach considerably reduces the computational cost of creating solar radiation maps over a large geographical area. However, due to the unique characteristics of the viewshed calculation process, it is necessary to ensure that enough buffer area is allowed around each building to guarantee accounting for potential shadowing effects, even if that means including some of the features suggested earlier for elimination. As an illustration, if a bridge is close to a building, this bridge should be retained in the DEM for solar radiation estimation analysis because such structure could impact the solar potential for that building.

3.2. The acquisition of the LiDAR data for the area of interest

Once the area of interest has been identified, the corresponding LiDAR data should then be obtained. Again, the resolution of the LiDAR data is very important for an accurate estimation of solar radiation. The accuracy of the LiDAR data should be fine enough for the results to be appropriate for practical implementations. LiDAR data must accurately reflect the unique characteristics of the rooftop, such as roof slope, roof orientation, and adjacent structures and vegetation useful in the modeling process. We found that LiDAR data with horizontal point spacing greater than 1 m typically do not reflect these characteristics.

3.3. The creation of the corresponding DEM data

The next step is to create two different LiDAR-derived data products: DEMs and building footprints. The actual creation of these products from the LiDAR data is a complex process, and the detailed description of their creation is beyond the scope of this paper. However, a brief overview is given for each LiDAR-derived product. The DEMs are three-dimensional representations of the surface of the earth obtained as a series of elevation values. DEMs are typically stored in a raster-based format consisting of millions of cells, with each cell representing an elevation value in relationship to the other cells in the raster. The higher the resolution of the LiDAR data, the greater the number of DEM cells. There are sets of commercial software for creating DEMs from LiDAR data including Qcoherent's LP360 (http://www.qcoherent.com/) and ArcGIS (http://www.arcgis.com).

Building footprints represent the outline of a given building, which in most cases is equivalent to the outline of its roof. The building outline makes it easier to determine the proportion of the roof area that is exposed to the sun. However, identifying only the building footprint is not sufficient for the modeling. A buffer distance must be incorporated to account for the surrounding features. There are several approaches for generating this data product. One approach involves manually digitizing the roof outlines. This approach is not suitable for applications with many buildings. Another approach involves identifying the centroid of each building roof and creating a buffer with a radius equivalent to the radius of the roof area. Again, the approach has limited application, and prone to error. The approach used in this paper involves using LiDAR data to generate the building footprint. Again, there is a set of commercial software that can be used for this purpose.

3.4. The estimation of the solar intensity values

Once all these pre-processing steps have been accomplished, the GIS-based spatial solar radiation model is applied to the DEM to generate the solar radiation estimations. At this stage in the methodology, it is possible to set parameters in the model to account for site-specific variables that impact solar radiation levels for a particular location, such as weather conditions and time of year. Careful selection of these parameters is vital for accurate modeling of solar radiation intensities. As a result, the area of interest should be defined in such a way that the area is homogeneous in terms of environmental and topographical factors. If the initial area of interest is too large to assume homogeneity, the area can further be broken into smaller, unique sub-areas for implementation purposes. This idea will not only make the computation run faster, but also guarantee the use of appropriate modeling assumptions.

3.5. The creation of the solar radiation map using building footprints

The final step in the methodology is the extraction of solar radiation values for individual rooftops. The objective of this step is to "map" the intensity and location of solar radiation falling specifically on rooftops. These rooftop maps are a helpful visualization of how solar radiation varies from one roof to another, as well as how it varies due to various micro-topographical features around each building. For instance, it is possible to see how a tall building adjacent to another building impacts the amount of solar radiation on that side of the roof of the shorter building.

The rooftop solar radiation map extraction process may be accomplished in several ways. The simplest method involves using building footprints to identify rooftops in the previously created solar radiation data. This process can be used to extract thousands of rooftop solar maps in a short time period; however, caution should be exercised when using building footprints for extraction as they do not always represent the shape and size of a rooftop outline. In addition, extraction using individual building footprints often includes common rooftop features such as HVAC equipment and chimneys in the rooftop solar radiation map, which usually reduces the amount of roof area available for PV systems. However, with higher-resolution LiDAR data, areas around these rooftop features can be easily identified. A manual extraction of the rooftop areas is another method. This method, although highly refined when compared to extraction by building footprints, is labor intensive for a large number of buildings. As a result, it is most suitable for situations that require precise rooftop solar radiation maps and/or for a fewer number of buildings.

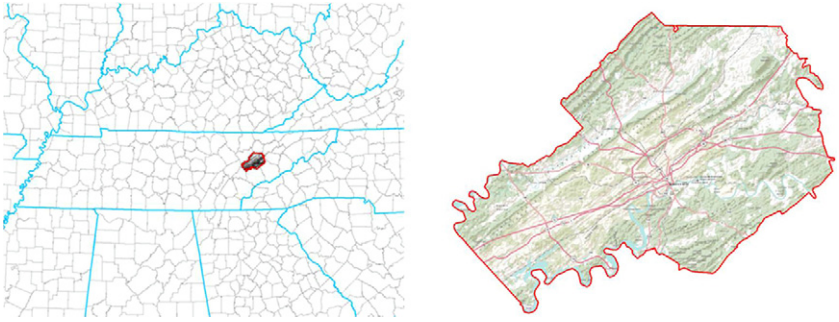

Fig. 7. Images showing the location and area of Knox County, Tennessee.

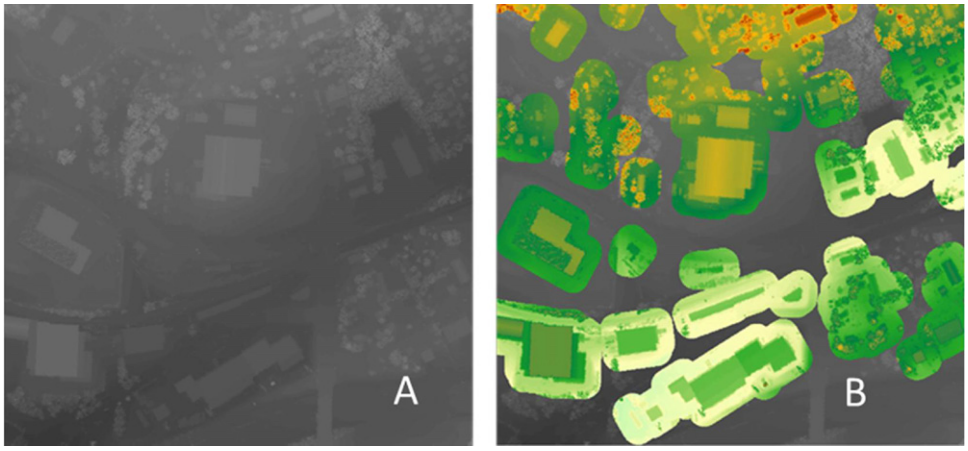

Fig. 8. The DSM for Knox County with no buffer (A) and with a 25-m buffer (B).

4. The implementation of the methodology for buildings in Knox County

To implement the methodology for buildings in Knox County, we acquired high-resolution LiDAR data for the entire county from the Knoxville Geographic Information Systems (KGIS) office. In addition to the raw LiDAR data, KGIS also provided a set of building footprints for approximately 212,000 pre-2004 buildings in the county. For the benefit of the readers, the location of Knox County in the state of Tennessee, USA and its area and boundary are shown in Fig. 7.

The creation of solar radiation raster data at a county scale presents some challenges due to the immense size of the datasets involved. Knox County has a surface area of approximately 526 square miles, and the corresponding DEM file size is over 10 gigabytes. So, the immediate decision was to eliminate portions of the DEM that are not required for computing rooftop solar radiation, and that could unnecessarily increase the computation time. To achieve this objective, we eliminate features, such as, roads, farmland, forest, grass, and pavement, from the data. In order to avoid eliminating features that could shadow the roofs, a 25-m buffer area is created around each building. The hope is that this buffer area will capture all the adjacent features around a building. Fig. 8 shows two images. The image "A" is the original DSM for an area, and image "B" shows the identified buildings in this area with a 25-m buffer around each building. The dark portions of image "B" that are without any buffer are subsequently eliminated in other to achieve speedy estimation of rooftop solar potential.

After the elimination of the unwanted features, the refined DEM for Knox County is shown in Fig. 9 (the right image). Comparing the overview images in Fig. 9 (image before (on the left) and after (on

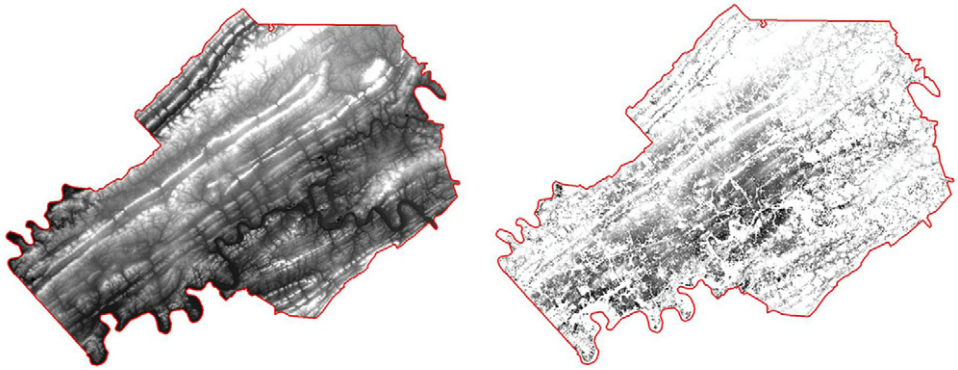

Fig. 9. The DEM for Knox County before (left) and after (right) the elimination of unwanted features.

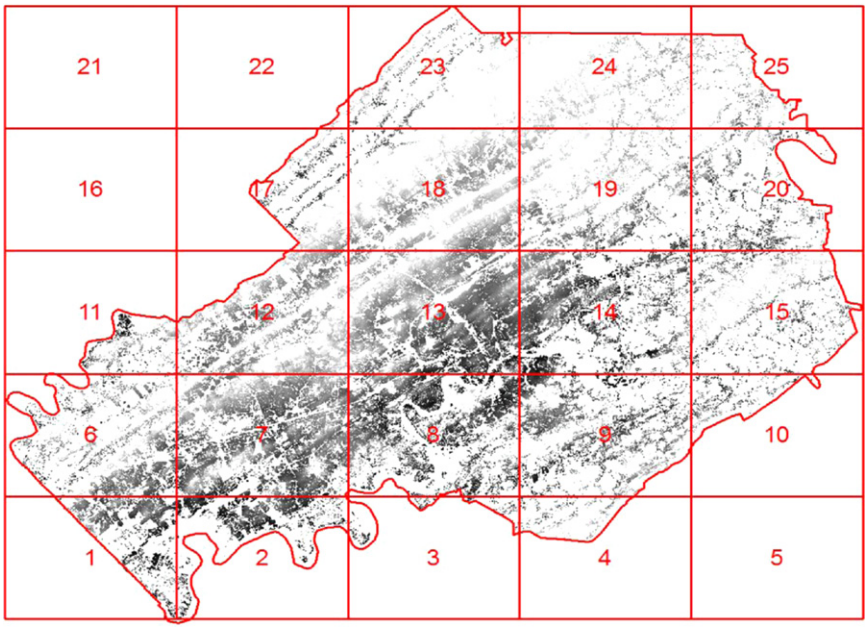

Fig. 10. The division of the Knox County area into smaller and manageable sizes.

the right) the elimination process), shows the effect of the elimination process.

With the elimination of unwanted features, the processing of the entire county in a single computer run was still a challenge; therefore, we also decided to minimize computation data by processing the data in batches or parallel. As a result, the entire county was divided into 25 raster tiles by using a 5 by 5 grid of smaller and manageable sizes as shown in Fig. 10. However, only 22 tiles actually overlap with the county boundary. Each raster tile is processed separately on multiple computers or in batches using the proposed methodology. The results are combined later for obtaining a solar radiation map for the entire county.

After the pre-processing steps, we used the area-based spatial solar radiation model in ArcGIS to create a series of monthly solar radiation maps using the refined DEM data. In order to account for monthly weather patterns, the solar radiation values were computed using monthly area-specific values that reflect the average atmospheric attenuation at the county level. The resulting extraction process created a series of monthly solar radiation maps for every rooftop in the county. Fig. 11 shows a schematic implementation of the framework for part of a residential subdivision in Knox County.

Fig. 11a shows the area of interest (in this case a sub-division). The corresponding refined DEM is shown in Fig. 11b; Fig. 11c is the outputs of the building footprint extraction as described in Section 3. The rooftop outlines are identified using the building footprints; these outlines are shown in Fig. 11d. The solar radiation estimation for this area of interest is shown in Fig. 11e; this includes the solar radiation value for the buffer area. Fig. 11f shows the corresponding solar radiation outputs for the extracted building footprints.

4.1. Visualization of and insights from building rooftop solar potential data

Rooftop solar radiation maps are a powerful way to show both the geographic distribution and intensity of solar radiation on a

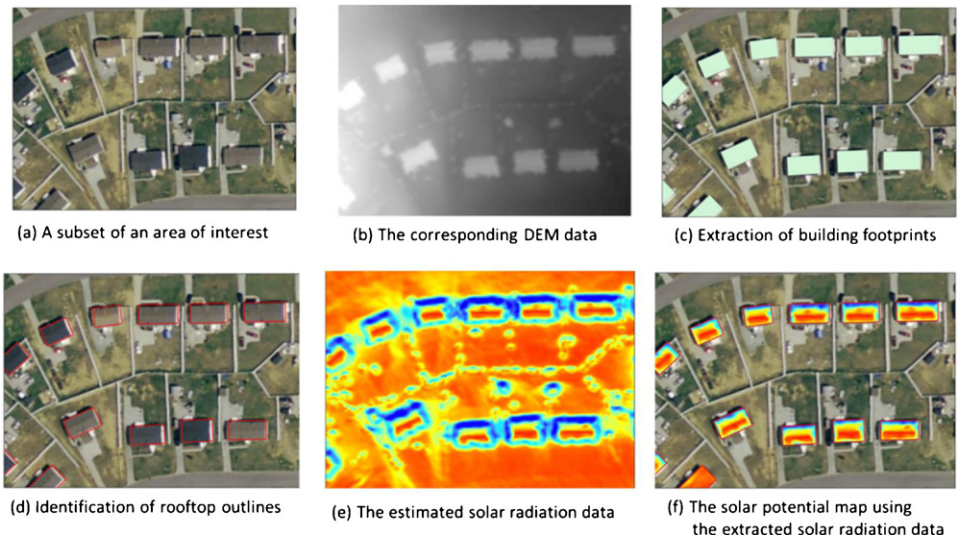

Fig. 11. The sequence of implementation of the methodology.

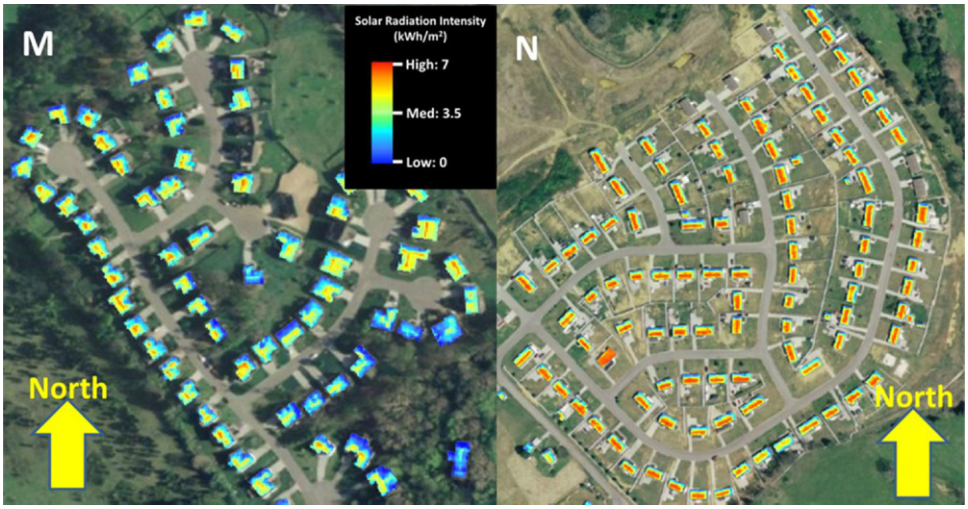

Fig. 12. A comparison of solar radiation estimations for two different residential subdivisions. (For interpretation of the references to color in the text, the reader is referred to the web version of the article.)

rooftop. The rooftop maps show what portions of each rooftop receive the highest levels of solar radiation. Looking at the image in Fig. 11f, one can see that the south-facing parts of the roof have higher potential than the north-facing part of the roof. Likewise, the rooftop solar radiation results display as maps also show portions of the roof shaded by taller trees or adjacent buildings. This is especially the case for some of the residential buildings shown in Fig. 12 (image M). The portions of the roof in blue are areas shaded by adjoining trees. One can immediately see the difference in solar radiation values between portions of the roof without adjacent trees (for example, image "N") and portions of the roof surrounded by trees (some of the buildings in image "M").

The shading impact of adjacent vegetation actually raises future research opportunities. Typically, home owners plant trees to shade their houses in order to minimize their energy consumption. However, if a home owner is considering a PV application, there is a need to determine the optimum distance and height for any surrounding trees in order to eliminate partial shading of the roof, but trees should be tall enough to provide some shading for the doors and windows. To demonstrate this insight, the image "N" in Fig. 12 shows the solar radiation estimation for a recently developed subdivision with no trees around the homes. Comparing this image to image "M" in Fig. 12, one can immediately see the impact of large trees on rooftop solar potential.

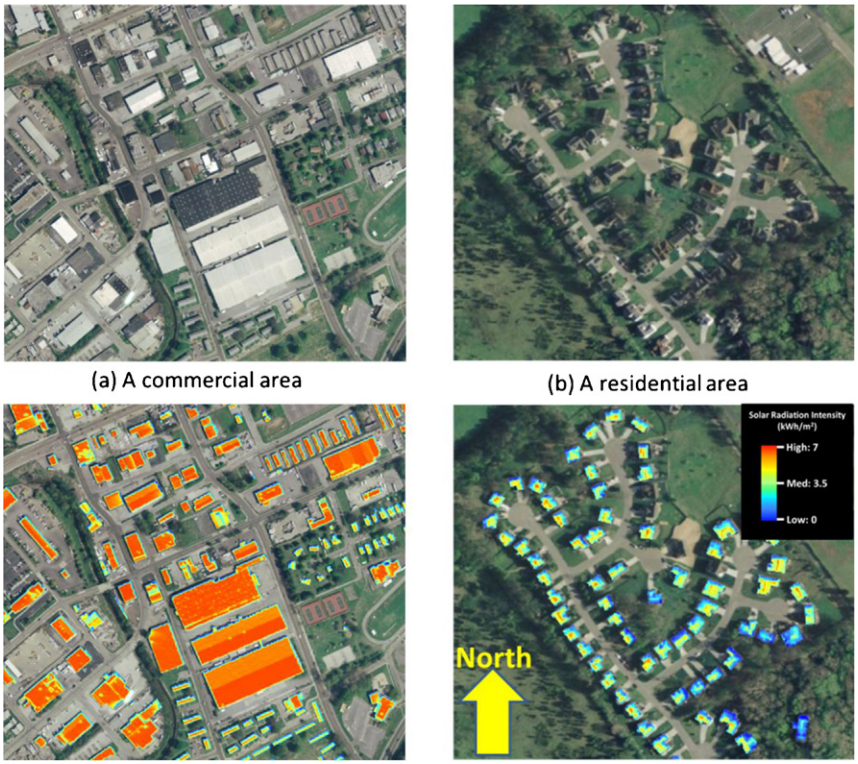

Fig. 13. Demonstrating the difference in solar radiation values between residential and commercial roofs. (For interpretation of the references to color in the text, the reader is referred to the web version of the article.)

Additional insight is demonstrated by considering the two most common roof types encountered in Knox County – commercial and residential building roofs. Aerial images of these two types of rooftops areas are shown in the top images in Fig. 13. The corresponding solar radiation maps are shown in the bottom images in Fig. 13; the red color denotes the highest solar radiation intensity, blue color denotes the least solar radiation intensity, and yellow color is between blue and red.

Additional insight is that the use of even higher resolution LiDAR data could further help to obtain more accurate results, since all features surrounding each building would be completely characterized. This will further minimize uncertainty in estimation solar radiation potentials.

4.2. Initial validation of the results

The best approach to validate the results of our model is to use ground-truth data from either pyranometers solar radiation measuring equipment or installed solar PV systems. We are currently collaborating with some local electric utilities and residential customers with installed solar PV for some field data to use for this purpose. In the meantime, we decided to use observed solar radiation values from standardized meteorological stations for validation. This approach will allow us to have some understanding of the overall accuracy of the methodology, pending the availability of some ground truth data.

For our comparison, we used the observed solar radiation data from the National Solar Radiation Data Base (NSRDB). The NSRDB is a national source of 30 years of solar radiation and supplementary meteorological data from 237 national weather stations. The associated data, available at http://rredc.nrel.gov/solar/old_data/nsrdb/, offers monthly summaries of solar radiation values in kilowatt hours per meter square per day for various surface orientations. The comparison of our results to the observed data from a weather station in Knoxville is shown in Fig. 14.

From Fig. 14, it appears that the methodology creates a pattern of monthly values that correspond to the NSRDB values. However, some interesting patterns were discovered in the verification process that warrants further discussion. One interesting patterns are the results for the winter-time. There are discrepancies between the wintertime NSRDB values and our results. According to the NSRDB data, the average solar radiation in January is about 2.2 kWh/m^2/day (Dataset-1), while it is about 1.6 kWh/m^2/day based on our method using varying transmissivity value (Dataset-2) and about 1.2 kWh/m^2/day using a constant value for the transmissivity (Dataset-3). Interestingly, these differences in values are most pronounced in the winter-time, while it is relatively negligible in the summer-time. The solar radiation value for July from NSRDB and our model is about 6.1 kWh/m^2/day. The same observation is true for the month of June. In all cases, our model estimates closely the solar radiation values in the spring and summer months, but slightly under estimate in the winter months. Based on these results, we uncover two insights. On the one hand, the results confirm that a correct transmissivity value is important for accurate estimation of solar radiation values. This is more important in the winter months. The use of ground-truth data should help further confirm this statement. On the other hand, the correct estimation of solar radiation values are location dependent, therefore, the use of observed data at weather stations is approximation of the actual solar radiation values for areas that are not closer to the weather station. Hence, the best validation data would be the use of ground-truth data. As a result, we are exploring the use of ground-truth data for further validation. Even then, the results of the validation discussed in this paper show that our model is a good approximation for estimating solar radiation values on building rooftops.

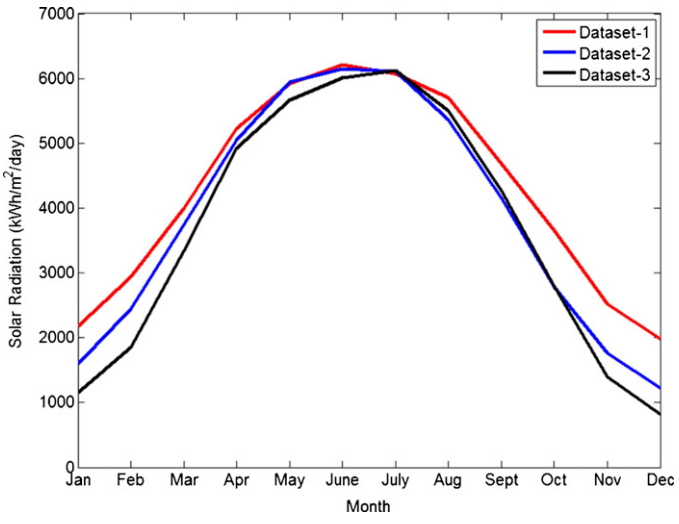

Fig. 14. Comparison of the monthly average solar radiation intensity (no tilt) for a representative location in Knox County, Tennessee.

5. Conclusions

As a result of the challenges in obtaining solar radiation values for individual buildings in a city for photovoltaic applications, we presented a method for estimating solar radiation values for multiple buildings in a city. The method combines high-resolution DEM data with upward-looking hemispherical viewshed algorithm to account for the unique variables that influence solar radiation potential for a particular building. This method has been demonstrated to work effectively for creating building rooftop solar radiation maps at a city scale by applying it to approximately 212,000 buildings in Knox County, Tennessee, USA.

The rooftop solar radiation maps obtained from the method outlined in this paper provide better estimations of individual building solar radiation potential than simply taking a building roof area and multiplying it by the solar radiation average for the region the building is located. The reason for the better estimation is because it accounts for building specific characteristics as well as possible shading agents that may be present. The results can further help users easily identify portions of the roof with high solar potential. While some of the results obtained have been verified using data from measuring instruments, there is still some work to be done in performing additional validation of the results. We are currently working with local utilities and home owners with installed PV to obtain some actual data for validation purposes.

In addition to application for individual home owners, the results could further be used by utilities to identify groups of buildings with enough solar potential for utility-scale distributed generation. Such an application could help utilities in setting up their distributed generation, while postponing expensive distribution infrastructure expansion. A further research in this area is on-going using techniques such as mean-variance portfolio (MVP) theory for selecting buildings with sufficient solar potential.

The quantification and mapping of rooftop solar potential at a city scale could play an important role in reducing the uncertainty associated with estimating potential electricity yield on buildings. It provides a quick and effective estimation resource for communities and utilities interested in energy sustainability. The methodology developed in this paper could help communities and utilities achieve this objective.

Acknowledgments

This manuscript is authored by employees of UT-Battelle, LLC, under contract DE-AC05-00OR22725 with the U.S. Department of Energy. Accordingly, the United States Government retains and the publisher, by accepting the article for publication, acknowledges that the United States Government retains a non-exclusive, paid-up, irrevocable, world-wide license to publish or reproduce the published form of this manuscript, or allow others to do so, for United States Government purposes.

References

ArcGIS Help Library. (2011a). *Area solar radiation (Spatial Analyst)*. ArcGIS Resource Center. Accessed on 01.11.2011 from: http://resources.arcgis.com/en/help/main/10.1/index.html#//009z000000t5000000

ArcGIS Help Library. (2011b). *Creating raster DEMs and DSMs from large LiDAR point collections*. ArcGIS Resource Center. Accessed on 20.10.2011 from: http://help.arcgis.com/en/arcgisdesktop/10.0/help/index.html#//00q80000006m000000

Adnan, S., Arcaklioglu, E., Ozalp, M., & Caglar, N. (2005). Forecasting based on neural network approach of solar potential in Turkey'. *Renewable Energy*, *30*(7), 1075–1090.

CH2MHill. (2008). *CH2MHill Solar Automated Feature Extraction™ Technology*. Online at http://www.ch2m.com

Elminir, H. K., Azzam, Y. A., & Younes, F. I. (2007). Prediction of hourly and daily diffuse fraction using neural network, as compared to linear regression models. *Energy*, *32*, 1513–1523.

Fu, P., & Rich, P. M. (2000). *The solar analyst 1.0 user manual*. Helios Environmental Modeling Institute, LLC. Accessed on 13.05.2010 from: http://www.fs.fed.us/informs/solaranalyst/solar_analyst_users_guide.pdf

Gadsden, S., Rylatt, M., & Lomas, K. (2003). Putting solar energy on the urban map: A new GIS-based approach for dwellings. *Solar Energy*, *74*, 397–407.

Gaisma. (2011). *Gaisma climate website for Knoxville, Tennessee*. Accessed on 10.07.2011 from: http://www.gaisma.com/en/location/knoxville-tennessee.html

Hammer, A., Heinemann, D., Hoyer, C., Kuhlemann, R., Lorenz, E., Muller, R., et al. (2003). Solar energy assessment using remote sensing technologies. *Remote Sensing of Environment*, *86*, 423–432.

Hoff, J. L. (2009). *The expanding role of the roof*. Presented at Construct 2009. Accessed on 18.06.2011 from: http://www.roofingcenter.org/syncshow/uploaded_media/CONSTRUCT_20092.pdf

Hofierka, J., & Kanuk, J. (2009). Assessment of photovoltaic potential in urban areas using open-source solar radiation tools. *Renewable Energy*, *34*, 2206–2214.

López, G., Batlles, F. J., & Tovar-Pescador, J. (2005). Selection of input parameters to model direct solar irradiance by using artificial neural networks. *Energy*, *30*, 1675–1684.

Mellit, A., Benghanem, M., Hadj Arab, A., & Guessoum, A. (2005). A simplified model for generating sequences of global radiation data for isolated sites: Using artificial neural network and a library of Markov transition matrices. *Solar Energy*, *79*(5), 468–482.

Mubiru, J., & Banda, E. J. K. B. (2008). Estimation of monthly average daily global solar irradiation using artificial neural networks. *Solar Energy*, *82*(2), 181–187.

Neteler, M., & Mitasova, H. (2004). *Open source GIS: A GRASS GIS approach* (2nd ed.). Boston: Kluwer Academic Publishers.

Sen, Z., & Sahin, A. D. (2001). Spatial interpolation and estimation of solar irradiation by cumulative semivariograms. *Solar Energy*, *71*(1), 11–21.

Suri, M., & Hofierka, J. (2004). A new GIS-based solar radiation model and its application to photovaoltaic assessments. *Transactions in GIS*, *8*(2), 175–190.

Suri, M., Huld, T. A., & Dunlop, E. D. (2005). PV-GIS: A web based solar radiation database for the calculation of PV potential in Europe. *International Journal of Sustainable Energy*, *24*, 55–67.

Suri, M., Huld, T. A., Dunlop, E. D., & Hofierka, J. (2007). Solar resource modeling for energy applications. In R. J. Peckham, & G. Jordan (Eds.), *Digital terrain modeling, development and applications in a policy support environment* (pp. 259–273). Berlin, Heidelberg: Springer.

Tymvios, F. S., Jacovides, C. P., Michaelides, S. C., & Scouteli, C. (2005). Comparative study of angstroms and artificial neural networks methodologies in estimating global solar radiation. *Solar Energy*, *78*, 752–762.

Wilson, J. P., & Gallant, J. C. (2000). Secondary topographic attributes. In J. P. Wilson, & J. C. Gallant (Eds.), *Terrain analysis: Principles and applications* (pp. 87–132). New York: John Wiley and Sons.